Influence of Cell Deformation on Leukocyte Rolling Adhesion in Shear Flow

X. Lei
Bioengineering Program,
The Pennsylvania State University,
University Park, PA 16802

M. B. Lawrence
Department of Biomedical Engineering,
University of Virginia,
Charlottesville, VA 22908

C. Dong
Bioengineering Program,
The Pennsylvania State University,
University Park, PA 16802
Mem. ASME

Blood cell interaction with vascular endothelium is important in microcirculation, where rolling adhesion of circulating leukocytes along the surface of endothelial cells is a prerequisite for leukocyte emigration under flow conditions. HL-60 cell rolling adhesion to surface-immobilized P-selectin in shear flow was investigated using a side-view flow chamber, which permitted measurements of cell deformation and cell–substrate contact length as well as cell rolling velocity. A two-dimensional model was developed based on the assumption that fluid energy input to a rolling cell was essentially distributed into two parts: cytoplasmic viscous dissipation, and energy needed to break adhesion bonds between the rolling cell and its substrate. The flow fields of extracellular fluid and intracellular cytoplasm were solved using finite element methods with a deformable cell membrane represented by an elastic ring. The adhesion energy loss was calculated based on receptor-ligand kinetics equations. It was found that, as a result of shear-flow-induced cell deformation, cell–substrate contact area under high wall shear stresses (20 dyn/cm^2) could be as much as twice of that under low stresses (0.5 dyn/cm^2). An increase in contact area may cause more energy dissipation to both adhesion bonds and viscous cytoplasm, whereas the fluid energy input may decrease due to the flattened cell shape. Our model predicts that leukocyte rolling velocity will reach a plateau as shear stress increases, which agrees with both in vivo and in vitro experimental observations.

Introduction

Circulating leukocyte emigration from vasculature into tissues, the central event in inflammation, is responsible both for the successful host defense against tissue infection and for many inflammatory disorders. Through extensive studies in recent years, it has become clear that at least four distinct steps act in sequence to regulate this event: (*i*) selectin-carbohydrate mediated initial leukocyte tethering and rolling; (*ii*) activation of integrins on leukocyte surfaces; (*iii*) transition from rolling to sticking via cell spreading; (*iv*) arresting of activated leukocyte and its adhesion to endothelial cells. Following the guidance of chemo-attractants, leukocytes then cross the endothelial lining and enter the tissues (Springer, 1994).

Members of the selectin family mediate leukocyte rolling on vascular endothelium. There are three known selectin molecules: L-, E-, and P-selectin. For example, P-selectin (also known as CD62, GMP140, or PADGEM) is stored in the Weibel–Palade body of endothelial cells and can be mobilized to the cell membranes within minutes of endothelial stimulation by agonists such as thrombin and histamine. Consequently, P-selectin can be up-regulated on the endothelial cell surface during the early stages of an inflammatory response. *In vitro* and *in vivo* studies have suggested that leukocyte rolling on a selectin was a prerequisite for integrin-mediated firm adhesion, especially under shear stress (Lawrence and Springer, 1991; von Andrian et al., 1991; Moazzam et al., 1997). Anti-P-selectin monoclonal antibody was successfully used *in vivo* to attenuate reperfusion injury involving P-selectin mediated adhesion (Winn et al., 1993).

While much has been learned regarding the molecular mechanisms required for leukocyte rolling adhesion, it is still not fully understood how hemodynamic force and leukocyte rheological properties regulate leukocyte rolling on vascular endothelium. Quantitative *in vivo* measurements indicated that initially the velocity of rolling leukocytes increased linearly with blood flow velocity but showed no further increase after blood velocities were greater than 1600 μm/s (Atherton and Born, 1973). Due to difficulties in characterizing both hemodynamic force acting on rolling leukocytes and expression level of adhesion molecules on vascular endothelium *in vivo,* parallel-plate flow chambers have widely been used to study leukocyte adhesion under flow conditions (Lawrence et al., 1987). However, information about leukocyte deformation and adhesion contact area is not easily obtained using this method. In the present study, a side-view flow chamber (Cao et al., 1997) was used to measure leukocyte deformation, adhesion contact length, and leukocyte rolling velocity.

Using simple dimensional analyses, a robust framework has been developed to model leukocyte rolling in terms of energy gain and loss (Schmid-Schoenbein et al., 1987). An alternative leukocyte rolling model based on force and momentum balance was developed without considering deformation of the rolling leukocyte (Tozeren and Ley, 1992). Other studies showed that leukocyte deformation might greatly influence the shear force and adhesion force acting on rolling leukocytes (House and Lipowsky, 1988; Firrell and Lipowsky, 1989). Drawing on these previous works and a biophysical adhesion model (Dembo et al., 1988), a two-dimensional leukocyte rolling model has been developed in this study to predict leukocyte deformation, adhesion contact length, and leukocyte rolling velocity using both finite element method (FEM) and finite difference method (FDM).

Materials and Methods

Human promyelocytic leukemic cell lines (HL-60) were maintained in a suspension of RPMI 1640, supplemented with 10 percent fetal bovine serum (FBS), L-glutamine (0.292 mg/ml), penicillin (100 U/ml), and streptomycin sulfate (100 μg/ml) (Biofluid, Rockville, MD). The cells were kept at 37°C with 5 percent CO_2 in a humidified tissue culture incubator. For flow assays, HL-60 cells were resuspended in HBSS (supplemented with 1 mM Mg^{2+}, 1.2 mM Ca^{2+}, 10 mM HEPES, pH 7.4). To

Contributed by the Bioengineering Division for publication in the JOURNAL OF BIOMECHANICAL ENGINEERING. Manuscript received by the Bioengineering Division September 3, 1998; revised manuscript received July 21, 1999. Associate Technical Editor: S. P. Sutera.

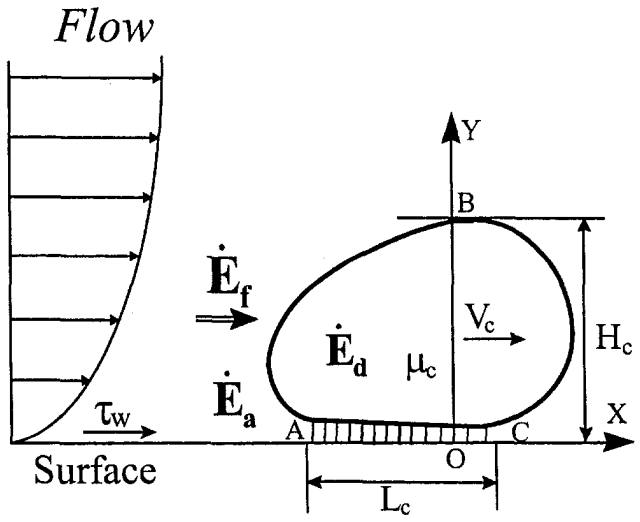

Fig. 1 A two-dimensional model of leukocyte rolling under conditions of flow. $\dot{E}_f$ is the rate of energy provided by the surrounding fluid to the rolling cell; $\dot{E}_a$ is the rate of energy dissipated during the adhesion bonds disruption; $\dot{E}_d$ is the rate of energy loss due to cytoplasm viscous dissipation; τ_w is the inlet wall shear stress; μ_c is the cytoplasmic viscosity; v_c is the cell rolling velocity; H_c is the height; L_c is the contact length.

increase cell deformability, HL-60 cell suspensions were incubated with 10 μM cytochalasin B (CB) (Sigma, St. Louis, MO) at 37°C for 10 min before the flow assay.

The side-view flow chamber consisted of two precision rectangular glass tubes called microslides (Cao et al., 1997). The smaller microslide was inserted into a larger one to create a flow channel with a flat surface on which the selected adhesion molecules were present. Two optical prisms, each with a 45 deg chromium-coated surface, were used along the flow channel to generate side-view light illumination. This design allowed the measurement of cell rolling velocity, cell shape change, and cell–substrate contact length.

P-selectin was purified from outdated blood platelets by immunoaffinity chromatography (Lawrence et al., 1997). Prior to P-selectin adsorption, the smaller microslides were first cleaned in an ultrasonic cleaner, then thoroughly washed in distilled water and again with deionized water. The air dried microslides were then stored in 100 percent ethyl alcohol. P-selectin molecules were adsorbed to the microslide surface by soaking the microslides in P-selectin solution for 2 hours. Nonspecific adhesion sites were blocked with 2 percent human serum albumin (HSA, Red Cross, Swiss) 30 minutes before experiments. Site density of adsorbed P-selectin on the glass surface as a function of P-selectin solution concentration was determined by a radioimmunoassay using a functional blocking monoclonal antibody G1 (Lawrence et al., 1997). Unlike other types of experiments on the cell-surface interaction, continuous cell rolling often happened with certain substrate ligand densities. Higher and lower P-selectin densities did not show to support a continual rolling (Lawrence and Springer, 1991). For this reason, two selected seeding densities (375 and 530 sites/μm^2) were chosen in the current study based on the strength of adhesion and the degree of cell deformation. The chosen densities would simulate an average expression of P selectin present on the cytokine-activated endothelium.

HL-60 cell suspension was perfused through the flow channel over the P-selectin immobilized substrate using a syringe pump (Harvard Apparatus, South Natick, MA). The rolling adhesion of HL-60 cells on P-selectin was observed through an inverted microscope (Nikon, Melville, NY) and captured by a CCD camera (Dage MTI, Michigan City, IN) mounted on the microscope. These images were recorded for analysis. The effects of flow conditions (wall shear stress τ_w from 0.5 to 20 dyn/cm^2), cell deformability (untreated and CB-treated) and substrate P-selectin density (375 and 530 sites/μm^2) on HL-60 cell deformation and rolling velocity were analyzed.

Theoretical Considerations

To understand the relative influence of shear flow, adhesion strength, and cell deformability on leukocyte rolling, a two-dimensional model was employed (Fig. 1). Although leukocyte membrane and cytoplasm could contain viscous or viscoelastic components, a steady-state rolling leukocyte was represented in a simplest way here by an elastic ring enclosing an incompressible viscous fluid. Adhesion bonds formed between leukocyte surface and its substrate were treated as elastic springs that were perpendicular to the substrate. Cell rolling velocity, v_c, was calculated based on the energy rate balance, assuming that the rate of energy provided by the surrounding fluid to the rolling cell ($\dot{E}_f$) dissipated predominantly into two parts: (1) $\dot{E}_a$, energy dissipation due to adhesion bond separation; and (2) $\dot{E}_d$, energy loss due to cytoplasm viscous dissipation (Schmid-Schoenbein et al., 1987). Other energy gains and losses from biochemical sources during bond association and dissociation were neglected:

$$\dot{E}_f = \dot{E}_a + \dot{E}_d \tag{1}$$

Cell membrane and its underneath actin-rich cortical layer were simulated by a prestressed elastic ring. When the fluid–solid coupling problem was resolved, the nonadherent elastic ring deformed under both extracellular and intracellular fluid stresses. The deformation of adherent part under the adhesion force was calculated coupling with adhesion bond kinetics (Dembo et al., 1988). Using curvilinear coordinates (s, s,ϕ) of the membrane (Fig. 2), the balance of forces normal and tangent to the cell surface were:

$$T\phi' = -q$$

$$T' = -t \tag{2}$$

where q and t were normal and tangential components of the fluid stresses (nonadherent part) or bond force (adherent part), respectively, and T was the membrane tension. The prime (') indicates the differential d/ds. These equations were solved using the Runge–Kutta–Verner method (IMSL Math. Library: IVPRK).

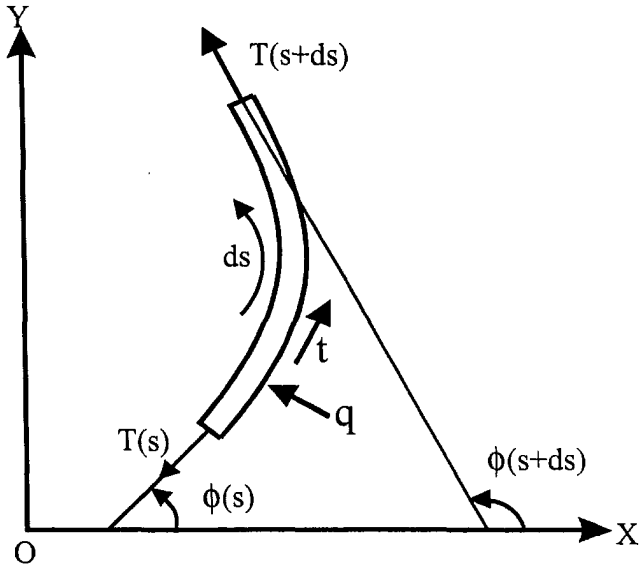

Fig. 2 Coordinates and forces involved in membrane deformation. T is the membrane tension; q and t are the normal and tangential components of the surface stresses, respectively; s is the arc coordinate; ϕ is the angle between a tangent drawn from a point on the ring to the substrate.

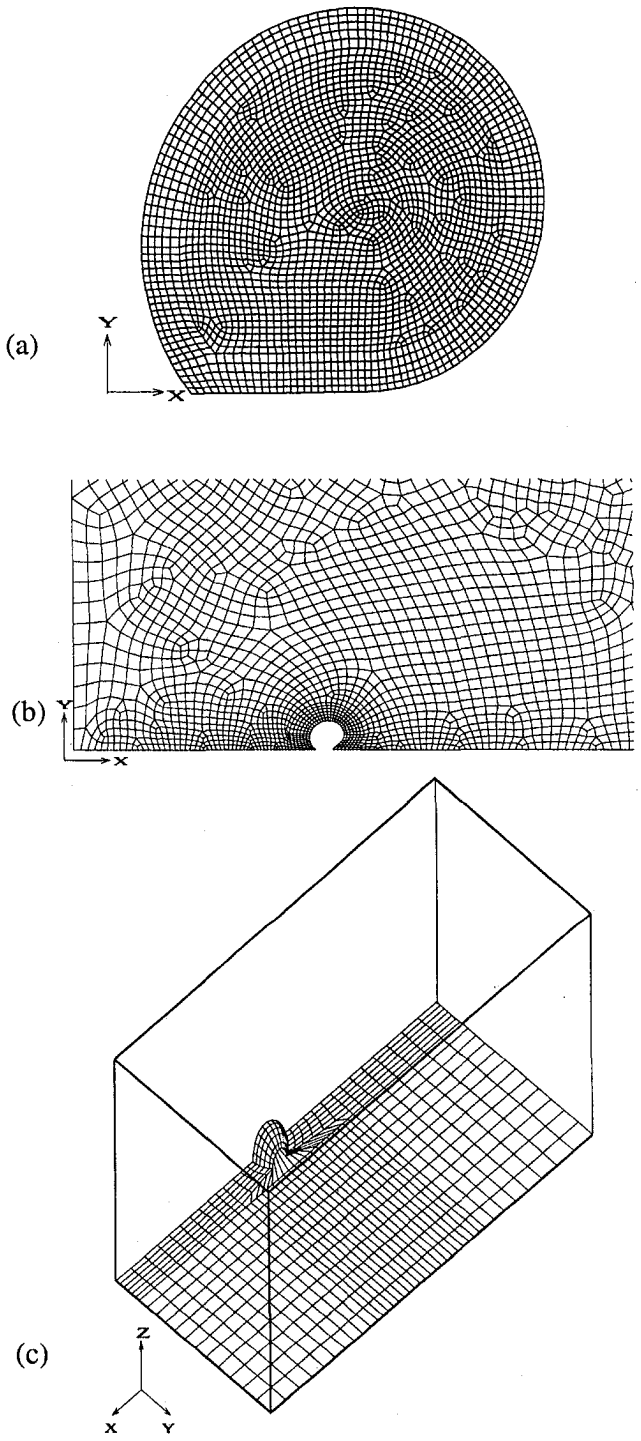

Fig. 3 A typical two-dimensional finite element mesh used for the flow field generated by FIDAP: (*a*) inside a rolling cell; (*b*) outside a rolling cell; (*c*) a three-dimensional FIDAP mesh on the bottom of the flow channel and the surface of an adherent cell

The intracellular and extracellular flow fields were calculated using a finite element analysis package (FIDAP, Fluid Dynamics International). It was assumed that fluid surrounding the cell membrane and fluid enclosed by the cell membrane were homogeneous, incompressible, and Newtonian (with different viscosities). Finite element methods were used to solve the two-dimensional steady-state Navier–Stokes equations. Figures 3(*a, b*) show a typical two-dimensional mesh inside and around a rolling cell generated by FIDAP. For intracellular mesh, the mesh generator was able to make an evenly distributed mesh along the cell membrane, except at the corners where the rolling cell began or ended contact with the substrate. For the extracellular flow field, the entrance and exit lengths were chosen to be respectively 15 and 25 times the undeformed cell radius. The entrance flow was a fully developed two-dimensional Poisseuille flow. At the surface of the lower and upper boundaries of the flow channel and of the rolling cell, no slip and no penetration conditions were assumed. The penalty function approach was used to eliminate the pressure as an unknown from the Navier–Stokes equations. The main idea was that the continuity equation would be set to be equal to a very small value epsilon ($\nabla \cdot v = -\epsilon P$, $\epsilon = 10^{-6}$) instead of zero. Then the variable pressure could be deleted from the Navier–Stokes equations (FIDAP: Tutorial 10.6 and Theory 5.3). Convergence was assumed when the norm of both residual vector and solution vector were less than 10^{-5}. The intracellular flow field was solved similarly, with no slip and no penetration boundary conditions for the inner surface of cell membrane. A flow field around a three-dimensional adherent cell was then calculated as an indication to show any difference in two-dimensional model. Based on the method developed by Cao et al. (1998), Fig. 3(*c*) shows the mesh on the bottom of the flow channel and the cell surface generated by FIDAP.

The rate of energy provided by the flow ($\dot{E}_f$) to the rolling cell was:

$$\dot{E}_f = \iint_{S_f} \sigma_{ij} \nu_j v_i dS = w_c \cdot \int_{C_f} \sigma_{ij} \nu_j v_i ds \tag{3}$$

where S_f is the surface exposed to the flow field; C_f is the corresponding two-dimensional circumference; σ_{ij} is the fluid stress; ν_j is the normal unit vector of the surface; and v_i is the velocity on the surface. On the assumption of cell volume conservation, an effective cell width of $w_c = 4R_c/3$ was derived (R_c was the radius of an undeformed cell, which was 6 μm for an average HL-60 cell).

The rate of energy dissipation of the viscous cytoplasm ($\dot{E}_d$) became,

$$\dot{E}_d = \int_V \sigma_{ij} \epsilon_{ij} dV = w_c \cdot \int_S \sigma_{ij} \epsilon_{ij} dS \tag{4}$$

where V is the cell volume, S is the cell cross-sectional area in the two-dimensional model, and ϵ_{ij} is the strain rate.

Adhesion kinetics equations were solved coupling with membrane equations. The adhesion bond force was assumed to be $f_b = N_b k(y - \lambda)$, where N_b is the bond density, k is the bond (P selectin—PSGL-1 pair) elastic constant, λ and y are the lengths of an unstretched bond and a stretched bond, respectively.

$$0 = v_c \frac{\partial N_b}{\partial s} + k_f(N_l - N_b)(N_r - N_b) - k_r N_b \tag{5}$$

$$k_f = k_{feq} \exp\left(\frac{-k_{ts}(y - \lambda)^2}{2B_z}\right) \tag{6}$$

$$k_r = k_{req} \exp\left(\frac{(k - k_{ts})(y - \lambda)^2}{2B_z}\right) \tag{7}$$

In Eqs. (5)–(7), N_l is the ligand (P-selectin) density on the substrate; N_r is cell surface receptor density; k_{feq} and k_{req} are forward and reverse reaction rate constant for unstretched bonds; k_{ts} is the bond elastic constant in transient state; B_z is thermal energy. The associated bond density $N_b(s, \phi)$ would be solved within the domain of the contact area (for a two-dimensional case, it would be the contact length L_c). Therefore, N_b will be directly related to the contact length L_c. Cell rolling velocity v_c corresponds to membrane peeling velocity v_{pl} at the trailing edge of cell-surface contact (Dembo et al., 1988), which is different from v_i in Eq. (3). The surface velocity v_i was defined as the fluid

Table 1 Parameters used in theoretical calculations (Dembo et al., 1988; Hammer and Apte, 1992)

Symbol	Definition	Used value
N_r	Total receptor density (sites/cm^2)	$2x10^{10}$
N_l	Total ligand density (sites/cm^2)	$3\sim6x10^{10}$
k_{feq}	Forward rate constant (cm^2/s)	$1x10^{-9}$
k_{req}	Reverse rate constant (1/s)	10.
k, k_{ts}	Bond elastic constant(dyn/cm)	0.5, 0.48
λ	Bond length (nm)	10.
B_z	Thermal energy (ergs)	$4x10^{-14}$

velocity on the cell surface, while the cell-rolling velocity v_c was defined as the moving velocity of a whole cell (i.e., the cell center velocity).

The energy loss in overcoming adhesion was proportional to adhesion bond force and cell rolling velocity:

$$\dot{E}_a = w_a \cdot \int_0^{L_c} f_b v_c \frac{\partial y}{\partial s} ds \tag{8}$$

with w_a the effective width of the contact area ($w_a = \pi L_c/4$, assuming a circular contact area).

Equation (1) must be met all time in terms of three energy rates, in order to calculate the correct cell-rolling velocity v_c, which was involved in all three energy rates represented by Eqs. (3), (4), and (8). Coupled with Eqs. (5)–(7), other unknown model parameters could be derived, such as intracellular viscosity μ_c, adhesion bond density distribution N_b, and membrane peeling y. All other employed parameters are listed in Table 1.

Results

Untreated and CB-treated HL-60 cells rolling on P-selectin were observed under wall shear stresses ranging from 0.5 to 20 dyn/cm^2. Typical side-view images of HL-60 cell rolling on P-selectin under low and high shear stresses are shown in Fig. 4(a). Cell shapes were calculated for various wall shear stresses as shown in Fig. 4(b), in which the model computed the equilibrium cell shapes (e.g., cell height H_c and contact length L_c). A criterion was based on converging iteration of cell membrane geometry with flow stresses calculated by FIDAP. H_c, L_c and cell rolling velocity v_c (Figs. 4(a, b)) were measured and calculated, as shown in Fig. 5(a–c). It is clearly shown that as inlet wall shear stress τ_w increases, rolling cells change their shapes from a nearly spherical to a more tear-drop appearance, resulting in a decrease in H_c and an increase in L_c. CB-treated HL-60 cells were found more deformable and hence had smaller H_c and larger L_c compared to untreated HL-60 cells. However, no significant change in H_c or L_c was seen for different P-selectin densities.

It was also found that cell rolled faster when they were under higher shear stresses or lower P-selectin densities (Fig. 5(c)). More deformable CB-treated HL-60 cells rolled at a slower velocity than untreated HL-60 cells with the same P-selectin density. As shear stresses increased, HL-60 cell rolling velocities gradually reached a plateau. Variation of P-selectin density and cell deformability had much greater influence under higher shear stresses. Theoretical predictions on HL-60 cell deformation and rolling velocity were compared with the experimental measurements (Fig. 5(a–c)) to estimate values for cytoplasmic viscosity and the adhesion bond reaction rate constants. Other parameters were applied based on previous studies by Dembo et al. (1988) and Hammer and Apte (1992) as listed in Table 1.

The rate of fluid energy from the surrounding fluid to the rolling cell and the percentage of adhesion and cytoplasmic energy dissipation rate are presented in Fig. 6(a–c). In general, the rate of fluid energy $\dot{E}_f$ increased with an increase in shear stress, where adhesion bonds consumed more than 80 percent (viscous cytoplasm consumed less than 20 percent) of the rate of fluid energy. As shear stresses increased, $\dot{E}_a/\dot{E}_f$ decreased, in spite of an increase in the absolute amount of adhesion energy loss $\dot{E}_a$. In comparison, both $\dot{E}_d$ and $\dot{E}_d/\dot{E}_f$ increased as shear stresses increased, indicating a relative strong influence of cytoplasm viscous dissipation on cell rolling adhesion under high shear stresses.

From calculations, the maximum shear stress acting on a rolling cell surface (two-dimensional) was found to be 2–6 times of the inlet wall shear stress, strongly depending on cell deformability and channel dimensions. Cell–substrate contact length L_c increased from 7.49 μm to 9.50 μm, as the channel height H reduced from 100 μm to 20 μm. For the same H change, the cell height H_c changed from 10.9 μm to 10.2 μm. The influence of channel height H on shear stress distributions on the surfaces of rigid spheres and deformable cells is shown in Fig. 7(a). The maximum shear stress τ_{max} (Point C) on the surface of deformed cells was considerably lower than that on rigid spheres, which was more

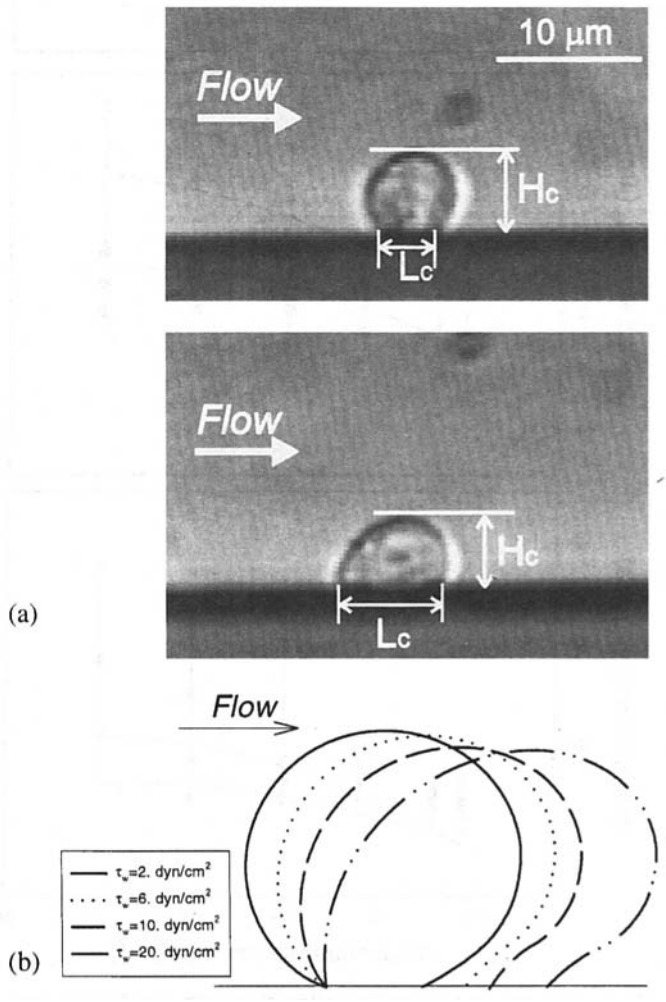

Fig. 4 (*a*) *In vitro* side-view images of rolling HL-60 cells on a P-selectin (375 sites/μm^2) coated substrate under shear stresses of 2 dyn/cm^2 (top) and 15 dyn/cm^2 (bottom), respectively. Flow channel height was about 500 μm. (*b*) Typical cell shapes calculated under various wall shear stresses using model parameters listed in Table 1. Cell membrane tension T was estimated to be 0.012 dyn/cm with a cytoplasmic viscosity μ_c around 50 poise.

apparent for a smaller channel. It would be anticipated with some differences between two-dimensional and three-dimensional calculations. Figure 7(*b*) shows shear stress distributions on an adherent cell surface, illustrating a very similar trend to the two-dimensional case (Fig. 7(*a*)). However, the τ_{max} on the three-dimensional adherent cell surface was found about two times the inlet wall shear stress, which was lower than τ_{max} from a two-dimensional calculation using a similar channel height H.

The maximum shear stress τ_{max} on a cell surface (two-dimensional) was found slightly decreased when H decreased, but

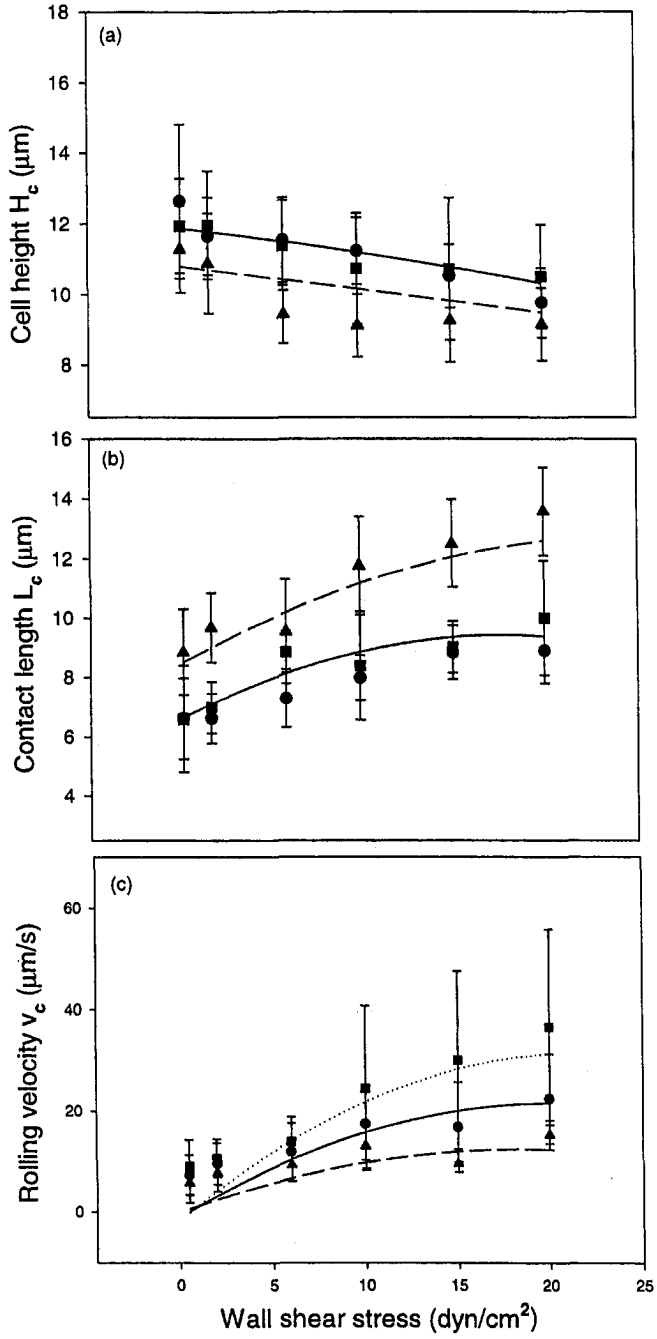

Fig. 5 Comparison of theoretical calculations with experimental measurements on HL-60 cell rolling (flow channel height = 500 μm): (*a*) cell height; (*b*) cell–substrate contact length; (*c*) cell rolling velocity. Dots represent experimental data and lines represent theoretical calculations. Symbols ● and solid lines are for untreated cells, N_l = 530 sites/μm^2, μ_c = 50 poise; symbols ■ and dotted lines are for untreated cells, N_l = 375 sites/μm^2 μ_c = 50 poise; symbols ▲ and dashed lines are for CB-treated HL cells, N_l = 530 sites/μm^2, μ_c = 40 poise.

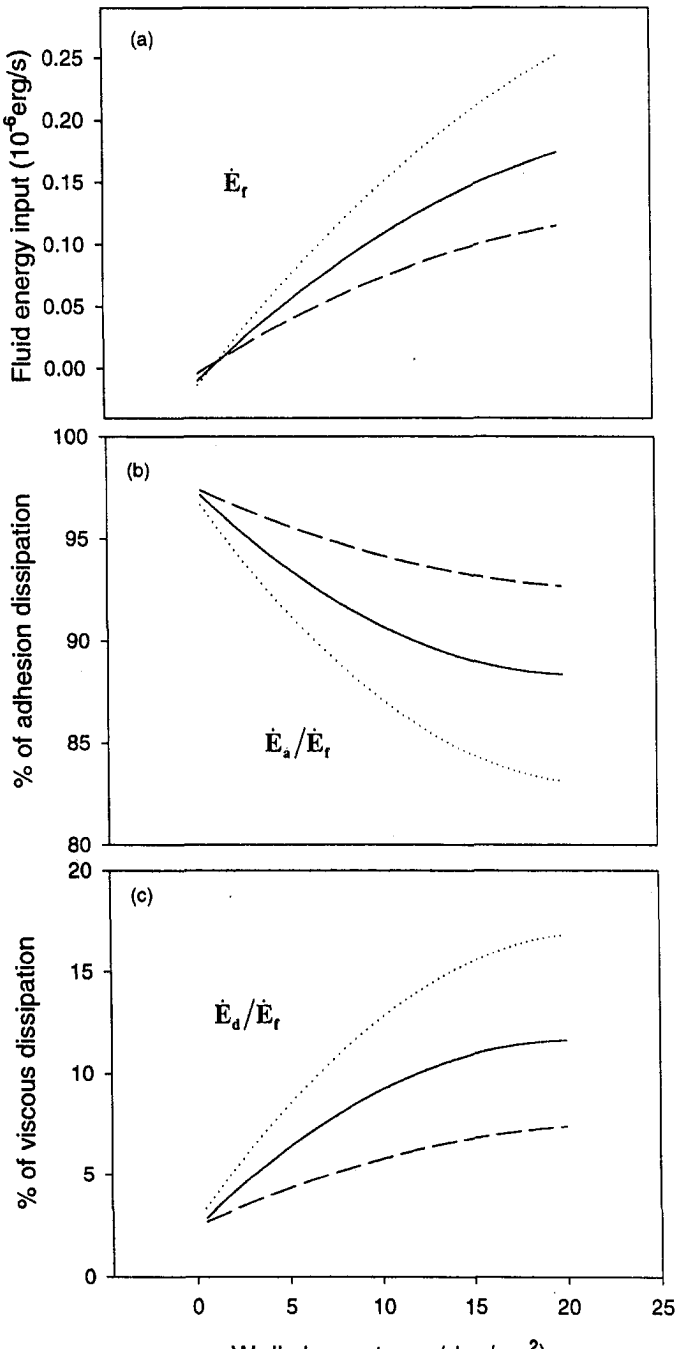

Fig. 6 Ligand density and cell deformability effects on: (*a*) fluid energy rate: $\dot{E}_f$; (*b*) percentage of adhesion dissipation in fluid energy input: $\dot{E}_a/\dot{E}_f$, (*c*) percentage of cytoplasmic viscous dissipation in fluid energy input: $\dot{E}_d/\dot{E}_f$. Solid lines are for untreated cells with N_l = 530 sites/μm^2, μ_c = 50 poise; dotted lines are for untreated cells with N_l = 375 sites/μm^2 μ_c = 50 poise; dashed lines are for CB-treated cells with N_l = 530 sites/μm^2, μ_c = 40 poise.

increased rapidly when H became less than 50 μm with various shear stresses calculated (Fig. 8(*a*)). Fluid energy input and total drag force acting on the rolling cell followed a similar trend to τ_{max}. The influence of flow shear stress on cell rolling velocity was also calculated with various channel heights as shown in Fig. 8(*b*), and compared with previously published *in vivo* data on cell rolling from Firrel and Lipowsky (1989). Under low shear stresses (e.g., $\tau_w \leq 6$ dyn/cm^2), cell-rolling velocity steadily increased as shear stresses increased and was not significantly influenced by the channel height. However, there was a sensitive dependence of

cell-rolling velocity on decreased channel dimension under higher shear stresses ($\tau_w > 6$ dyn/cm^2), especially when $H < 50$ μm.

Cell deformation and cytoplasmic viscosity μ_c directly affect viscous dissipation, hence, the cell rolling velocity v_c. For example, as μ_c increased from very small values (1 poise to 50 poise), v_c decreased rapidly, particularly under high shear stresses (Fig. 9(*a*)). However, when μ_c was above 1000 poise, v_c decreased much less with a further increase in μ_c. On the other hand, adhesion kinetic parameters were also found to have a great impact on the cell-rolling velocity. Fig. 9(*b*) shows that for an ideal bond ($k = k_{ts}$), v_c was very small (<1 μm/s) and not sensitive to any changes in wall shear stress. As the adhesion bonds became more slippery ($k_{ts} < k$), the cell rolled faster (>100 μm/s). However, v_c still reached a plateau under higher shear stresses, indicating that a significant increase in cell deformation attenuated a further increase in cell rolling velocity.

Discussion

The objective of this paper was to present an *in vitro* side-view image system and a model to study how cell deformability influences shear flow-induced leukocyte rolling on endothelium.

For the experimental system, HL-60 cells were chosen because they had high levels of PSGL-1 (a ligand for P-selectin) expression, and similar mechanical properties to neutrophils (Moore et al., 1995). CB is a fungal agent that induces profound changes in cell morphology by inhibition of actin polymerization, and has been shown to increase the deformability of both leukocytes and HL-60 cells (Hallows and Frank, 1992; Tsai et al., 1996). Parallel-plate flow chambers have been widely used to study leukocyte adhesion under flow conditions. However, information regarding cell deformation and cell–substrate contact has been obviously difficult to obtain. Therefore, a side-view flow chamber, which allowed measurements of cell deformation and contact length (Cao et al., 1997), has been proven to be a useful tool to study leukocyte–endothelium adhesion in shear flow.

A two-dimensional model was presented to study the mechanics of cell-rolling adhesion in terms of cell deformation in shear flow. The importance of leukocyte deformation in leukocyte–endothelial interaction has not been adequately addressed partially because of difficulties in calculating whole cell deformation together with cell-surface adhesion, plus the shear flow dynamics. A model of undeformed rolling leukocytes was initially proposed by Tozeren and Ley (1992), which was innovative but limited to very low shear stresses (less than 2 dyn/cm^2). *In vivo* measurements (House and Lipowsky, 1988; Firrell and Lipowsky, 1989) suggested that cell deformation was remarkably large under high shear stresses, and this contributed to the plateaued cell rolling velocity as shear stress increased. As a result of shear flow-induced cell deformation, for example, cell–substrate contact area for CB-treated HL-60 cells under 20 dyn/cm^2 wall shear stress were twice of that under a low shear stress (0.5 dyn/cm^2).

It is noticed that the rolling motion of leukocytes fluctuates randomly. A stochastic model by Zhao et al. (1995) showed that experimentally determined rolling velocities depended on the time

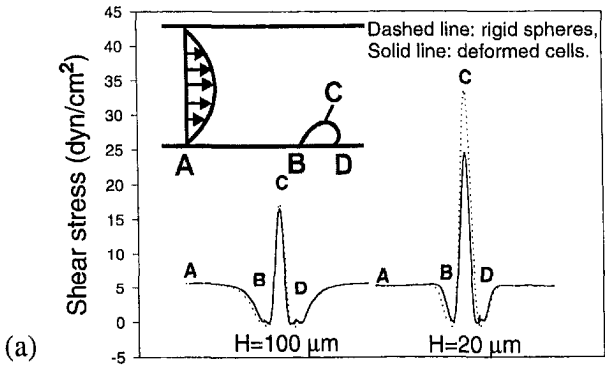

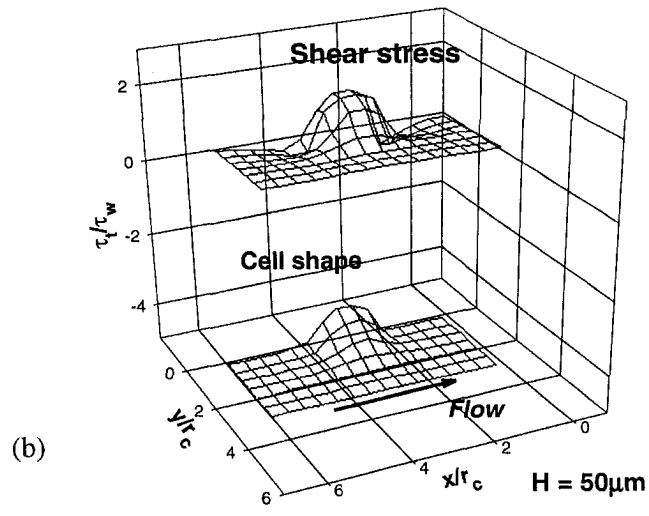

Fig. 7 (*a*) Effects of cell deformation on shear stress distributions along the surface of a rolling-rigid sphere and a rolling-deformable cell for different flow channel heights (H = 20 and 100 μm, respectively). Inlet wall shear stress τ_w = 6.0 dyn/cm^2. (*b*) Shear stress distributions on a three-dimensional adherent cell surface (half data are shown; Cao et al., 1998). Inlet wall shear stress τ_w = 6.0 dyn/cm^2. Channel height H = 50 μm.

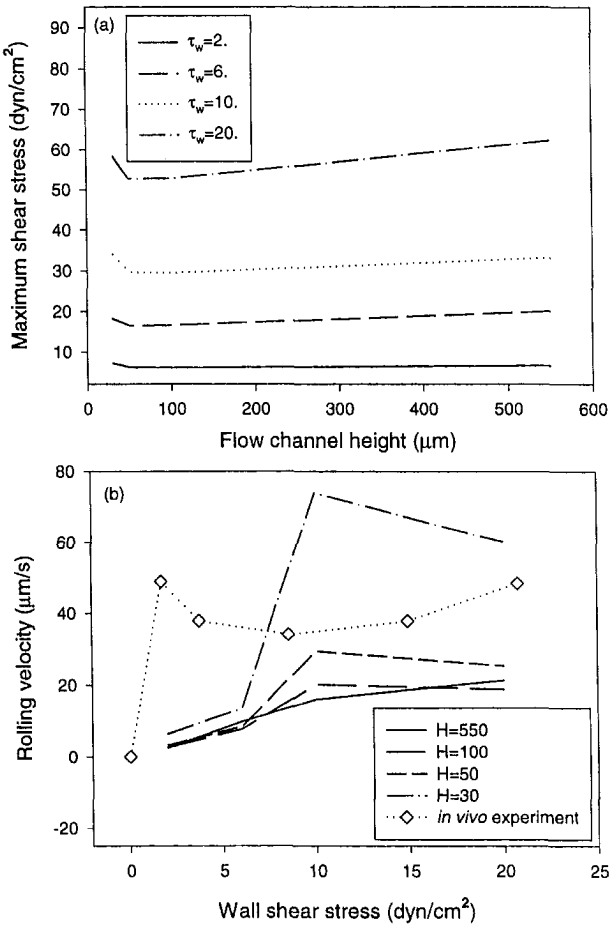

Fig. 8 (*a*) Effects of flow channel height on maximum shear stresses on a rolling cell surface under different inlet wall shear stresses (dyn/cm^2); (*b*) shear stress influence on cell rolling velocity (with N_l = 530 sites/μm^2, μ_c = 50 poise) under various flow channel heights (μm). *In vivo* data (via 30-μm-dia capillaries) were from Firrell and Lipowsky (1989).

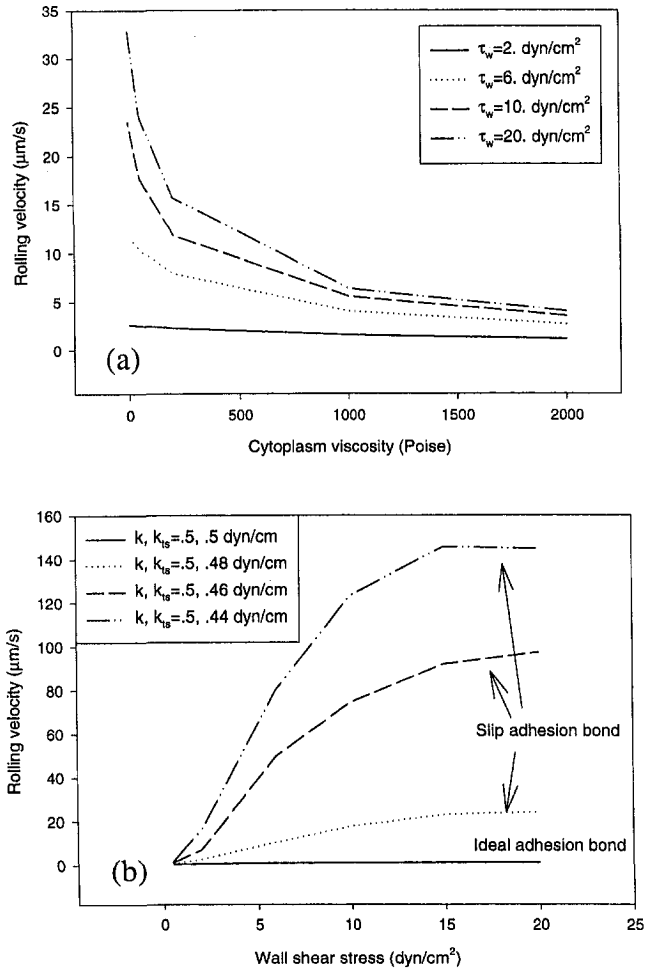

Fig. 9 (*a*) Effects of cytoplasmic viscosity on cell-rolling velocity with different inlet wall shear stress τ_w. k, k_{ts} = 0.5, 0.48 dyn/cm, respectively, and N_l = 530 sites/μm^2. (*b*) Influence of adhesion bond constants k and k_{ts} on cell rolling velocity with μ_c = 50 poise and N_l = 530 sites/μm^2.

Δt used in calculating velocities, since leukocyte rolling was a random process. However, with an averaged rolling leukocyte in mind, we are content at this stage with a deterministic mechanical approach to study the influence of shear flow-induced cell deformation on leukocyte rolling adhesion. Nevertheless, to illuminate the intriguing details of adhesion receptor–ligand interaction in this process, further studies from both approaches and better yet, combining both approaches in one, are really in need.

For the extracellular flow field computation, the cell surface has been assumed smooth in the current analysis, while it is actually ruffled and coated with numerous microvilli (length 0.2–2.0 μm). The main reason for a smooth membrane simplification was from the fact that the current two-dimensional model has already involved multiple parameters to take account for shear flow field, cell membrane, and cytoplasmic motion and cell-surface adhesion kinetics. An assumption of smooth cell surface may likely overestimate the actual cell-surface contact area by neglecting the microvilli. However, the obtained experimental images on cell-surface contact were unable to provide any further accuracy in cell contact area. Obviously, more sophisticated image techniques and cell membrane modeling will be needed to better simulate the cell rolling.

Changes in ligand (P-selectin) density did not show noticeable changes in cell deformation in terms of cell height H_c and contact length L_c (Fig. 5). CB-treated cells deformed more than untreated cells and consequently resulted in a smaller cytoplasm viscosity. With a larger ligand density, cells rolled more slowly and so did CB-treated cells compared with untreated cells. It was found that at a high shear stress, the influence of ligand density and cellular deformability on cell rolling velocity was greater than that at a low shear stress. As a result of energy distributions, $\dot{E}_d/\dot{E}_f$ becomes the biggest for the fastest rolling cells while $\dot{E}_a/\dot{E}_f$ has the maximum with the slowest rolling cells. In general, cell deformation would reduce the fluid energy to a cell because a flattened cell caused less disturbance to flow and hence smaller shear stress on the cell surface. Meanwhile, larger cell deformation would result in a large contact area and more adhesion energy needed to disrupt adhesion bonds, as well as a more disturbed cytoplasm flow field and more viscous dissipation. Therefore, cell deformation altered the dependence of the three energy rates on shear flow and contributed to a nonlinear dependence of cell rolling velocity on wall shear stresses.

The approach of a two-dimensional model should be expandable to a three-dimensional problem, when the three energy rates ($\dot{E}_f$, $\dot{E}_a$, and $\dot{E}_d$) are calculated for an actual three-dimensional situation accordingly with modifications on Eqs. (3), (4), (8). The main difficulties are how to simulate the three-dimensional cytoplasm flow field and three-dimensional membrane deformation numerically under fluid stresses. It would be simplified when all the integrals are reduced from three-dimensional to two-dimensional for the current analysis, while the results still share important insights in how cell deformability and cell–substrate adhesion affect cell rolling. Calculations on shear stress along a cell surface have not been found any significant discrepancies between the two-dimensional and three-dimensional cases (Fig. 7).

The influence of channel height H on the cell-rolling velocity was calculated and compared with an *in vivo* measurement. Due to limitations on available dimensions of microslides (the glass tubes), we were not able to vary the channel height in *in vitro* experiments now. It would require a right-fit dimension for a small rectangular glass tube to be inserted into a larger one to form the side-view flow channel (Cao et al., 1997). It was found that the rolling velocity of HL-60 cells exhibited a similar trend to an *in vivo* leukocyte, but plateau at a higher wall shear stress. Results in difference might reflect geometric differences between an *in vivo* capillary and an *in vitro* rectangular flow channel, or possible involvement of other adhesion molecules. Some other recent studies have also shown similar effects of flow channel height on the maximum shear stress and the cell-rolling velocity (Brooks and Tozeren, 1996; Gaver and Kute, 1998; von Andrian, 1997).

Cell deformation and intracellular viscosity directly affect the cytoplasmic viscous dissipation. As a rolling cell becomes more flattened (larger contact length) or cytoplasmic viscosity increases, more energy would be dissipated by the cytoplasm and result in a smaller rolling velocity. Some discrepancies might exist in estimating the values of intracellular viscosity μ_c (~45–1,500 poise) for leukocytes (Dong et al., 1988; Evans and Yeung, 1989; Lipowsky et al., 1991). It would be noted that the parameter μ_c is very "apparent" depending significantly on the method of evaluation, applied shear rates and degrees of cell deformation (Dong et al., 1991; Tran-Son-Tay et al., 1998). For example, when μ_c was above 1000 poise, a relatively low rolling velocity (less than 10 μm/s) was found (Fig. 9(*a*)), which was apparently less dependent on shear stresses. The μ_c values obtained in this study were derived from the best agreement with the experimental measurements on cell shapes, cell-surface contact length, cell rolling velocity, and various shear stresses. A general parametric trend for μ_c shown here provides important insights on how leukocyte rheological properties would affect cell rolling.

On the other hand, among various adhesion kinetic parameters, adhesion energy dissipation was found more sensitive with variations in adhesion bond constants k and k_{ts}. An ideal bond ($k = k_{ts}$) results in much slower cell rolling with less dependence on any changes in wall shear stresses. However, as the adhesion bonds become more slippery ($k_{ts} < k$), cells roll faster as shear stress increases, but reaching plateaus around 15 dyn/cm^2. The most recent work by Chen and Springer (1999) has also shown that wall shear stress increases the rate of dissociation of individual

selectin–ligand bonds, thereby destabilizing rolling. This would be compensated by a shear-dependent increase in the number of bonds per rolling step and hence an increase in adhesion energy dissipation.

In summary, shear-flow-induced leukocyte deformation could alter the balance between fluid driving energy, the adhesion bond energy and intracellular viscous energy in determining the leukocyte rolling mechanics. The stretching and elongation of a rolling cell in a shear flow tempers the hydrodynamic shearing force while provides larger contact area for adhesion force. Better experiment designs with the ability to measure those key parameters involved cell deformability and adhesion kinetics will be in great need to understand further how cell deformation influences leukocyte rolling under dynamic flow conditions.

Acknowledgments

This study was supported in part by the Whitaker Foundation grant and the NSF Career Award BES-9502069.

References

Alon, R., Hammer, D. A., and Springer, T. A., 1995, "Lifetime of the P-selectin-carbohydrate bond and its response to tensile force in hydrodynamic flow," *Nature,* Vol. 374, pp. 539–542.

Atherton, A., and Born, G. V. R., 1973, "Relationship between the velocity of rolling granulocytes and that of the blood flow in venules," *J. Physiol.,* Vol. 233, pp. 157–165.

Brooks, S. B., and Tozeren, A., 1996, "Flow past an array of cells that are adherent to the bottom plate of a flow channel," *Computers & Fluids,* Vol. 25, pp. 741–757.

Cao, J., Donell, B., Deaver, D. R., Lawrence, M. B., and Dong, C., 1998, "In vitro side-view imaging technique and analysis of human T-leukemic cell adhesion to ICAM-1 in shear flow," *Microvasc. Res.,* Vol. 55, pp. 124–137.

Cao, J., Usami, S., and Dong, C., 1997, "Development of a side-view chamber for studying cell-surface adhesion under flow conditions," *Ann. Biomed. Eng.,* Vol. 25, pp. 573–580.

Chen, S., and Springer, T., 1999, "An automatic braking system that stabilizes leukocytes rolling by an increase in selectin bond number with shear," *J. Cell Biol.,* Vol. 144, pp. 185–200.

Dembo, M., Torney, D. C., Saxman, K., and Hammer, D., 1988, "The reaction-limited kinetics of membrane-to-surface adhesion and detachment," *Proc. R. Soc. Lond. B,* Vol. 234, pp. 55–83.

Dong, C., Skalak, R., and Sung, K.-L. P., 1991, "Cytoplasmic rheology of passive neutrophils," *Biorheology,* Vol. 28, pp. 557–567.

Dong, C., Skalak, R., Sung, K.-L. P., Schmidt-Schoenbein, G. W., and Chien, S., 1988, "Passive deformation analysis of human leukocytes," ASME JOURNAL OF BIOMECHANICAL ENGINEERING, Vol. 110, pp. 27–36.

Evans, E., and Yeung, A., 1989, "Apparent viscosity and cortical tension of blood granulocytes determined by micropipet aspiration," *Biophys. J.,* Vol. 56, pp. 151–160.

FIDAP, 1993, "Fluid dynamics international," Version 7.0, Evanston, IL.

Firrell, J. C., and Lipowsky, H. H., 1989, "Leukocyte margination and deformation in mesenteric venules of rat," *Am. J. Physiol.,* Vol. 256, pp. H1667–H1674.

Gaver, D. P., III, and Kute, S. M., 1998, "A theoretical model study of the influence of fluid stresses on a cell adhering to a microchannel wall," *Biophys. J.,* Vol. 75, pp. 721–733.

Hallows, K. R., and Frank, R. S., 1992, "Changes in mechanical properties with DMSO-induced differentiation of HL-60 cells," *Biorheol.,* Vol. 29, pp. 295–309.

Hammer, D. A., and Apte, S. M., 1992, "Simulation of cell rolling and adhesion on surfaces in shear flow: general results and analysis of selectin-mediated neutrophil adhesion," *Biophys. J.,* Vol. 63, pp. 35–57.

House, S. D., and Lipowsky, H. H., 1988, "In vivo determination of the force of leukocyte-endothelium adhesion in the mesenteric microvasculature of the cat," *Circ. Res.,* Vol. 63, pp. 658–668.

IMSL, 1989, "Math/Library User's manual," Version 1.1, Houston, TX.

Lawrence, M. B., Kansas, G. S., Kunkel, E. J., and Ley, K., 1997, "Threshold levels of fluid shear promote leukocyte adhesion through selectins (CD62L, P, E)," *J. Cell Biol.,* Vol. 136, pp. 717–727.

Lawrence, M. B., McIntire, L. V., and Eskin, S. G., 1987, "Effect of flow on polymorphonuclear leukocyte/endothelial cell adhesion," *Blood,* Vol. 70, pp. 1284–1290.

Lawrence, M. B., and Springer, T. A., 1991, "Leukocytes roll on a selectin at physiologic flow rates: distinction from and prerequisite for adhesion through integrins," *Cell,* Vol. 65, pp. 859–873.

Lipowsky, H. H., Riedel, D., and Shi, G. S., 1991, "In vivo mechanical properties of leukocytes during adhesion to venular endothelium," *Biorheol.,* Vol. 28, pp. 53–64.

Moazzam, F., DeLano, F. A., Zweifach, B. W., and Schmid-Schonbein, G. W., 1997, "Leukocyte response to fluid stress," *Proc. Nat'l Acad. Sci. USA,* Vol. 94, pp. 5338–5343.

Moore, K. L., Patel, K. D., Bruehl, R. E., Li, F., Johnson, D. A., Lichenstein, H. S., Cummings, R. D., Bainton, D. F., and McEver, R. P., 1995, "P-selectin glycoprotein ligand-1 mediates rolling of human neutrophils on P-selectin," *J. Cell Biol.,* Vol. 128, pp. 661–671.

Schmid-Schoenbein, G. W., Skalak, R., Simon, S. I., and Engler, R. L., 1987, "The interaction between leukocytes and endothelium in vivo," *Ann. NY Acad. Sci.,* Vol. 516, pp. 348–361.

Springer, T. A., 1994, "Traffic signals for lymphocyte recirculation and leukocyte emigration: the multistep paradigm," *Cell,* Vol. 76, pp. 301–314.

Tozeren, A., and Ley, K., 1992, "How do selectins mediate leukocyte rolling in venules?" *Biophys. J.,* Vol. 63, pp. 700–709.

Tran-Son-Tay, R., Kan, H. C., Udaykumar, H. S., and Shyy, W., 1998, "Rheological modeling of leukocytes," *Medical & Biological Engineering & Computing,* Vol. 36, pp. 246–250.

Tsai, M. A., Wauch, R. E., and Keng, P. C., 1996, "Changes in HL-60 cell deformability during differentiation induced by DMSO," *Biorheol.,* Vol. 33, pp. 1–15.

von Andrian, U. H., 1997, "A message for the journey: keeping leukocytes soft and silent," *Proc. Natl. Acad. Sci. USA,* Vol. 94, pp. 4825–4827.

von Andrian, U. H., Chambers, J. D., McEvoy, L. M., Bargatze, R. F., Arfors, K. E., and Butcher, E. C., 1991, "Two-step model of leukocyte-endothelial cell interaction in inflammation: distinct roles for LECAM-1 and the leukocyte β_2 integrins in vivo," *Proc. Natl. Acad. Sci. USA,* Vol. 88, pp. 7538–7542.

Winn, R. K., Liggitt, D., Vedder, N. B., Paulson, J. C., and Harlan, J. M., 1993, "Anti-P-selectin monoclonal antibody attenuates reperfusion injury to the rabbit ear," *J. Clin. Invest.,* Vol. 92, pp. 2042–2047.

Zhao, Y., Chien, S., and Skalak, R., 1995, "A stochastic model of leukocyte rolling," *Biophys. J.,* Vol. 69, pp. 1309–1320.